ACS APPLIED MATERIALS & INTERFACES

Research Article

Cite This: ACS Appl. Mater. Interfaces 2019, 11, 11904−11909

www.acsami.org

Electrospun Polyimide/Metal-Organic Framework Nanofibrous Membrane with Superior Thermal Stability for Efficient $PM_{2.5}$ Capture

Zhimin Hao,[†] Juntao Wu,[*,†] Chaolu Wang,[†] and Jingang Liu[*,‡]

[†]Key Laboratory of Bioinspired Smart Interfacial Science and Technology of Ministry of Education, School of Chemistry, Beihang University, Beijing 100191, P. R. China

[‡]Beijing Key Laboratory of Materials Utilization of Nonmetallic Minerals and Solid Wastes, National Laboratory of Mineral Materials, School of Materials Science and Technology, China University of Geosciences, Beijing 100083, P. R. China

Supporting Information

ABSTRACT: Particulate matter (PM) pollution is a serious threat to human health. Zeolitic imidazolate framework-8 (ZIF-8) is a kind of metal-organic framework, and ZIF-8 not only can capture $PM_{2.5}$ efficiently but also possesses excellent chemical and thermal stability. In this study, ZIF-8-modified soluble polyimide (PI) nanofibrous membranes were prepared via an electrospinning process. As a result, the PI-ZIF membrane shows high $PM_{2.5}$ filtration efficiency (up to 96.6 ± 2.9%), superior thermal stability (up to 300 °C), good transmittance, excellent mechanical properties, and low pressure drop. The prepared PI-ZIF membrane with excellent comprehensive property shows a promising application in $PM_{2.5}$ capture, especially in harsh conditions.

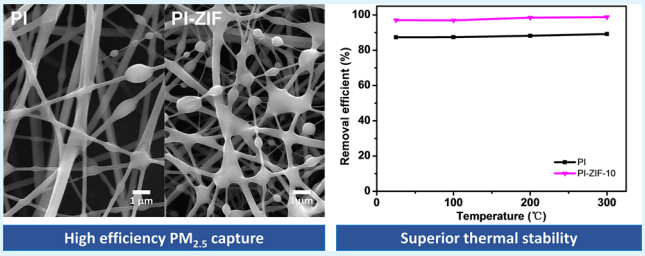

KEYWORDS: *polyimide, ZIF-8, air filtration, $PM_{2.5}$, high thermal stability*

1. INTRODUCTION

With the development of industries, air pollution, especially particulate matter (PM) pollution, has become a major environmental problem.[1−3] Compared with PM_{10}, $PM_{2.5}$ has a more serious adverse effect to human health.[4] Because of its small size, $PM_{2.5}$ can easily pass through the respiratory tract and even penetrate into the blood vessel. A growing evidence suggests that human long-term exposure to $PM_{2.5}$ pollution can increase the risk of cardiovascular and respiratory disease mortality.[5,6] The $PM_{2.5}$ removal filters are mainly divided into two types: the porous film filter and the fibrous filter, among which the latter is considered be more potential owing to its high surface area, light weight, low pressure drop, and facile synthesis.[7] However, the conventional fibrous filter has not been widely developed and applied owing to its inevitable drawbacks, such as low filtration efficiency, poor mechanical property, and bad thermal stability. Therefore, developing a novel filter material with excellent comprehensive property is a long-term goal for filtration material research.

ZIFs are a subclass of porous metal-organic frameworks (MOFs) with tetrahedral framework structures constructed from metal cations and imidazolate anions. Some ZIFs, such as ZIF-8, combine the attractive features of MOFs (large surface area, diversity of structure and pore, and functional tunability) and high thermal and chemical stability, which is rarely found among other MOF materials.[8−10] Recently, some studies have demonstrated that MOFs can achieve high-efficiency PM capture via their exceptional open metal sites, functional groups, and surface charges.[11,12] Polyimide (PI) as a high-performance material not only has excellent comprehensive performances, especially in mechanical properties and thermal stability, but also has high dipole moment (6.2 D), which indicates strong adhesion of PM on PI.[13−15] Besides, the existence of organic ligands in MOFs also makes them more compatible with polymers.[16]

Electrospinning is a fast and facile technology for preparing hybrid fibers. MOF/polymer fibers were successfully fabricated by electrospinning combined with direct blending or in situ growth.[17−21] Hence, we presented, for the first time, an electrospun polyimide/ZIF-8 (PI-ZIF) nanofibrous membrane for $PM_{2.5}$ capture application. We fabricated PI-ZIF membranes with different ZIF loadings, and their properties were systematically studied by X-ray diffraction (XRD), scanning electron microscopy (SEM), the Brunauer−Emmett−Teller (BET) test, thermogravimetric analysis (TGA), and the tensile test. Compared to that of the PI membrane, the filtration efficiency of PI-ZIF membranes is significantly enhanced. The highest $PM_{2.5}$ filtration efficiency of PI-ZIF membrane is 96.6 ± 2.9% with a 10 wt % ZIF loading. The PI-ZIF membranes also show superior thermal stability (up to 300 °C). Besides,

Received: December 28, 2018
Accepted: March 4, 2019
Published: March 4, 2019

DOI: 10.1021/acsami.8b22415
ACS Appl. Mater. Interfaces 2019, 11, 11904−11909

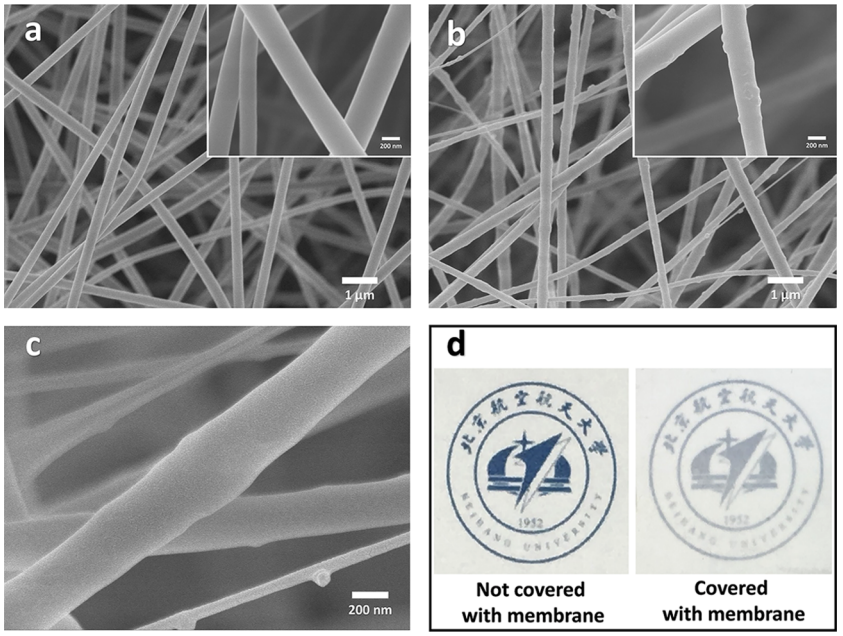

Figure 1. SEM images of PI-ZIF nanofibers (a) PI and (b, c) PI-ZIF-10. (d) Display of PI-ZIF-10 membrane transparency.

the obtained membranes show low pressure drop, good transmittance, and excellent mechanical properties. In short, the PI-ZIF membranes with excellent comprehensive property are promising materials for $PM_{2.5}$ capture, especially in harsh conditions.

2. EXPERIMENTAL SECTION

2.1. Materials. *N*,*N*-dimethylacetamide (DMAc), *N*,*N*-dimethylformamide (DMF), methanol, ethanol, acetic anhydride (Ac_2O), and pyridine were supplied by Beijing Chemical Works. 4,4′-(Hexafluoroisopropylidene)diphthalic anhydride (6FDA, CAS no. 1107-00-2) and 2,2′-bis[4-(4-aminophenoxy)phenyl]-hexafluoropropane (BDAF, CAS no. 69563-88-8) were supplied by Forsman Scientific(Beijing) Co., Ltd. Zinc nitrate hexahydrate ($(Zn(NO_3)_2{\cdot}6H_2O$, CAS no. 10196-18-6) and 2-methylimidazole (CAS no. 693-98-1) were purchased from Aladdin. All reagents are analytically pure. Of these reagents, except DMF and DMAc for which 4 Å molecular sieves were used to remove adsorbed water, all others were used as received.

2.2. Synthesis of Soluble Polyimide 6FDA−BDAF. The soluble polyimide (6FDA−BDAF) was synthesized via a two-step chemical imidization procedure, as illustrated in Figure S1. BDAF (5.185 g) and 54.6 g of DMAc were added to a three-necked flask equipped with a stirrer, an ice−water bath, and a nitrogen inlet. After BDAF was completely dissolved, 4.442 g of 6FDA was added into the mixture, producing a solution with 15 wt % solid content. The mixture was stirred for 1 h, removed from the ice−water bath, and stirred continuously at room temperature for 20 h. Then, the chemical imidization was carried out with Ac_2O (5.1 g) as a dehydrating agent and pyridine (4.0 g) as a catalyst at room temperature for another 20 h. The obtained viscous solution was carefully poured into excess of ethanol to yield a silky resin. The resin was collected and dried at 80 °C in vacuum for 24 h (yield, ∼95%).

2.3. Synthesis of ZIF-8. ZIF-8 was synthesized according to a previous procedure.[22] $Zn(NO_3)_2{\cdot}6H_2O$ (1.291 g) and 1.621 g of 2-methylimidazole were dissolved in 50 mL of methanol, respectively. The latter solution was rapidly poured into the former solution under stirring. Then, stirring was stopped and the mixed solution was kept statically. After 24 h, the powders were separated from the milky dispersion by centrifugation and washing with methanol. The product was dried at 120 °C for 12 h. The X-ray diffraction (XRD) pattern of sample was almost identical to the simulated pattern of known structural data (Figure S2) that demonstrates the product is the ZIF-8 material.[23] As shown in Figure S3, as-synthesized ZIF-8 particles present isometric nanoparticles with sharp edges and a narrow size distribution. A statistical evaluation of 100 particles results in an average diameter of 95 nm.

2.4. Preparation of the PI-ZIF Membrane. ZIF-8 powder (0.01 g) was first dispersed in 2 g of DMF by ultrasonic treatment and then 0.4 g of soluble polyimide was added. Then, the mixture was mechanically stirred to form a homogeneous solution with a ZIF-8 loading of 2.5 wt %. The electrospinning solution with different ZIF-8 loadings (0, 2.5, 5, and 10 wt %) was prepared by changing the content of ZIF-8. To prepare an electrospun membrane, the electrospinning solution was added in plain plastic syringes connected by a metal nozzle with an inner diameter of 0.65 mm. Then, the solution was electrospun into a nanofiber and collected on an aluminum foil. The parameters of the electrospinning were set as follows: the distance between the spinneret and the collector of 15 cm, high-voltage power supply of 15 kV, volume feed rate of 0.5 mL/h subjected by air pressure, respectively, under humidity of <40% RH at ∼25 °C.

2.5. Details of Filtration Efficiency and Pressure Drop Measurement. The obtained membranes were artificially peeled to 2 μm. To measure the filtration efficiency, the peeled membranes and a nonwoven as support and the filter holder were assembled to form a filter. The filtration efficiency and pressure drop of membranes were measured using the setup shown in Figure S4, and the setup was connected to a $PM_{2.5}$ source ($PM_{2.5}$ concentration exceeds 300 μg/m^3). Then, an air pump forced the air through the filter at a constant flow rate and countermeasured the concentration of $PM_{2.5}$ in the airflow. The $PM_{2.5}$ filtration efficiency was calculated according to the following equation: $E = (C_0 - C)/C_0$, where C_0 and C are the concentrations of $PM_{2.5}$ in airflow without and with filtration, respectively. Meanwhile, the differential pressure meter detected the pressure drop on both sides of the membrane under a controlled airflow. The effective area of the filter used for testing is 288.9 mm^2, and the airflow rate is 2.5 L/min.

2.6. Characterizations. The crystal structure was investigated by powder X-ray diffraction (XRD, Shimadzu, XRD-6000). The morphology was observed by a scanning electron microscope (FEI, Quanta 250 FEG and JEOL, JSM-7500F). The energy-dispersive X-ray spectroscopy (EDX) was performed to detect element distribution in fibers. Before the observation, the samples were coated with gold. The BET measurements were performed on Micromeritics ASAP

DOI: 10.1021/acsami.8b22415
ACS Appl. Mater. Interfaces 2019, 11, 11904−11909

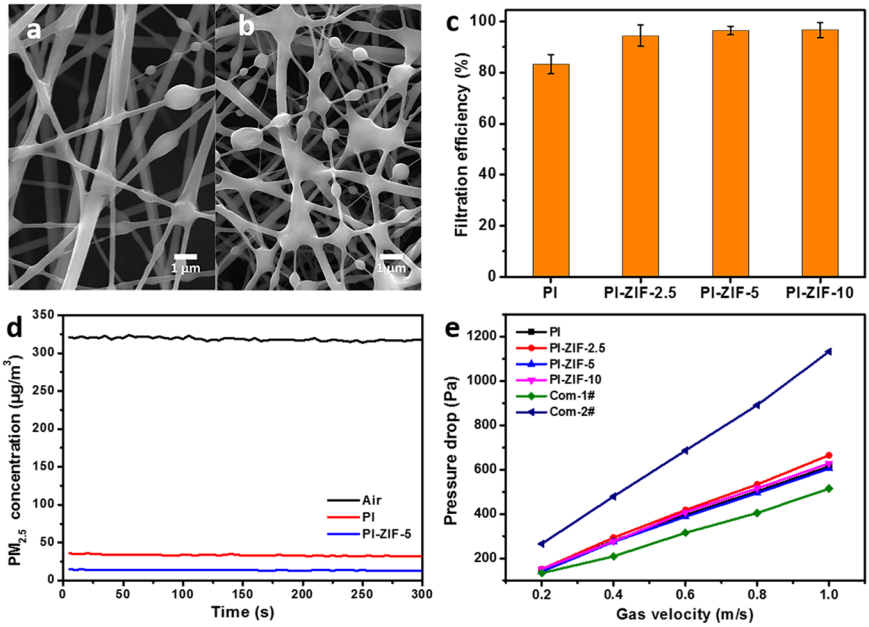

Figure 2. SEM images of PI (a) and PI-ZIF (b) membranes after filtration. (c) $PM_{2.5}$ filtration efficiency of different membranes. (d) $PM_{2.5}$ concentration after different membranes filtrating in real hazy environments. (e) Pressure drop of different membranes under different gas velocities.

2460. The mechanical property was tested by a Shimadzu AGS-X 1 kN universal mechanical testing machine. The thermal stability was investigated by a thermal analyzer (Netzsch, STA449F3). The mass concentration of the particle matter was determined using a TSI 8530 aerosol particle counter. The pressure drop of samples was detected by a differential pressure meter (Smart Sensor, AS510). The airflow through the membrane was measured by a gas flowmeter (SENLOO, MF5706).

3. RESULTS AND DISCUSSION

3.1. Characterization of the PI-ZIF Membrane. The PI-ZIF membranes were prepared using a single spinneret electrospinning technique under an ambient atmosphere. The nanofibrous membranes with different ZIF-8 loadings (0, 2.5, 5, and 10 wt %) were denoted PI, PI-ZIF-2.5, PI-ZIF-5, and PI-ZIF-10, respectively. Figure S5 shows the XRD pattern of PI-ZIF membranes with different ZIF-8 loadings. The (100) peak intensity of ZIF-8 in the XRD pattern increases with the increase of filler, indicating that the ZIF-8 particles were successfully incorporated in polyimide.[24,25] Upon addition of ZIF-8, some changes in fiber morphology were observed. Figure 1a,b displays the morphology of the as-spun PI-ZIF nanofibers. All of the examples exhibited an interconnected network formed by the random distribution of nanofibers with a diameter in the range of 200−300 nm. ZIF-8 particles were successfully introduced in PI fibers, and the particles dispersed uniformly in the matrix without apparent agglomeration. The uniform distribution of ZIF-8 was also confirmed by EDS element mapping (Figure S6). It is worth noting that the introduction of ZIF-8 changes the morphology of the fiber. The surface of the PI fiber was observed to be smooth (Figure 1a). Upon addition of ZIF-8, many protrusions appeared on the surface of the fiber and the surface became rough (Figure 1b). This change of surface roughness was mainly attributed to the introduction of ZIF-8 particles. Some ultrathin fibers with diameters less than 50 nm appeared after the ZIF-8 particles were added. The introduction of ZIF-8 particles changes electrical and surface properties of solution, which lead to further splitting of the jet and form ultrathin fibers.[26,27] As shown in Figure 1c, in those ultrathin fibers, the ZIF-8 particle can even connect to the fiber with a very small contact area. The BET was applied to measure the surface area of the material. The BET surface area of pure PI is 9.44 m^2/g, whereas the BET surface area of PI-ZIF-10 is 27.78 m^2/g. Both the porosity of ZIF-8 and the change of morphology can increase the surface area of the material. Among these, the latter can provide more adsorption sites for $PM_{2.5}$ capture.[28] In addition, the logo covered with a membrane peeled to 2 μm can still be clearly observed, indicating its good transmittance (Figure 1d).

3.2. $PM_{2.5}$ Filtration Performance of the PI-ZIF Membrane. Filtration efficiency is an important property that directly reveals the ability of a material for $PM_{2.5}$ capture. In this study, we choose cigarette smoke as the $PM_{2.5}$ source, which is a good model system for air filtration as it contains a large amount of $PM_{2.5}$ particles and some components are similar to real $PM_{2.5}$ pollution.[29] Figure 2a,b shows the micromorphology of PI and PI-ZIF membranes after filtration. Upon addition of ZIF-8, more $PM_{2.5}$ contaminants adhered onto the fiber and the morphology of contaminants changed from uniform wrapping to spindle under the effect of surface tension.[30] The filtration efficiencies of the membranes with different ZIF loadings of 0, 2.5, 5, and 10 wt % were 83.2, 94.4, 96.4, and 96.6% (Figure 2c), respectively. Obviously, the introduction of ZIF-8 can significantly improve the ability of the fiber for $PM_{2.5}$ capture. The improvement of fibers' capture ability may be caused by the following mechanisms: (1) surface charge of ZIF-8 enhanced the adhesion of $PM_{2.5}$ onto the fibers;[11] (2) rough morphology provides more adsorption sites for $PM_{2.5}$ capture; and (3) high adhesion effect of the ultrathin fiber to $PM_{2.5}$. It is found that the membranes with different ZIF loadings have comparable filtration efficiency. Besides, we also tested the filtration efficiencies of PI and PI-ZIF-5 filters in real hazy environments. As shown in Figure 2d, the filtration efficiencies of PI and PI-ZIF membranes were

DOI: 10.1021/acsami.8b22415
ACS Appl. Mater. Interfaces 2019, 11, 11904−11909

89.7 and 95.9%, respectively, which were consistent with results obtained from a simulated environment. In a 5 min test process, the membranes maintain a constant filtration efficiency without reducing, which indicates that the membrane is suitable for real hazy conditions.

Pressure drop is another important parameter to evaluate the filter performance. Generally, filtration efficiency and pressure drop are tradeoffs. The comprehensive performance of the filter combined filtration efficiency and pressure drop can be evaluated by quality factor (QF), $QF = -\ln(1 - E)/\Delta P$, where E is the filtration efficiency and ΔP is the pressure drop.[31,32] The pressure drops of the membranes with different ZIF-8 loadings of 0, 2.5, 5, and 10 wt % were 69, 69, 73, and 72 Pa, respectively, and their QFs were 0.0258, 0.0417, 0.0454, and 0.0470 Pa^{-1}, respectively. All of the membranes show a comparable pressure drop, whereas the PI-ZIF membrane has higher QF, which indicates that the PI-ZIF membrane has more excellent $PM_{2.5}$ interception ability. Figure 2e shows the pressure drop of the PI-ZIF and commercial filters as a function of gas velocity.[33,34] The values of pressure drop for all PI-ZIF filters fall in between those for the two different commercial filters, which means that PI-ZIF filters have an acceptable pressure drop. The detailed performances of different membranes are listed in Table 1. The result shows the PI-ZIF filters not only have high filtration efficiency for $PM_{2.5}$ but also have low pressure drop.

Table 1. Performance Summary of PI-ZIF Membranes

sample	E^a (%)	ΔP^b (Pa)	QF^c (Pa^{-1})	T^d (°C)
PI	83.2 ± 3.8	69 ± 1	0.0258	300
PI-ZIF-2.5	94.4 ± 4.2	69 ± 6	0.0417	300
PI-ZIF-5	96.4 ± 1.7	73 ± 1	0.0454	300
PI-ZIF-10	96.6 ± 2.9	72 ± 2	0.0470	300

[a]The $PM_{2.5}$ filtration efficiency. [b]The pressure drop at the flow rate of 0.144 m/s. [c]The quality factor. [d]The highest thermal stable temperature.

3.3. Thermal Stability of the PI-ZIF Membrane. The thermal stability of membranes under high temperature is also one of essential parameters that needs to investigate. Figure 3a shows the TGA curves of the PI, ZIF-8, and PI-ZIF-10 measured from room temperature to 900 °C under an air atmosphere. As shown in TG curves, the decomposition of ZIF-8 and polyimide occurred at 400 and 450 °C,[35,36] respectively. In addition, the thermal degradation of PI-ZIF-10 first appeared at 400 °C, which was in agreement to the decomposition temperature of ZIF-8. Both ZIF-8 and PI and their composites exhibited high thermal stability that can resist high temperature of above 300 °C. Hence, we have the reason to believe that the PI-ZIF filter can be applied to high-temperature conditions.

To further confirm the thermal stability of PI-ZIF membranes, we tested the filtration efficiency of the membranes after undergoing a process of high-temperature treatment and rapid cooling to simulate harsh conditions. Figure 3b presents the filtration efficiency of the PI-ZIF membrane after heat treatment at different temperatures. As expected, PI-ZIF membranes exhibited high filtration stability even at the heating treatment temperature of up to 300 °C. After undergoing heat treatment at 300 °C for 1 h, both the diameter and morphology of PI-ZIF-10 fibers were kept unchanged, as shown in Figure 3c,d. The thermal stability of ZIF-8 also verified by XRD measurement. As shown in Figure S2, ZIF-8, after heat treatment, still maintains the intrinsic crystallinity that indicates its high thermal stability. Very few studies have reported on $PM_{2.5}$ capture of the polymer/MOF composite material with such high thermal stability. The PI-ZIF membranes with high thermal stability provide a possible way for high-temperature PM filtration.

3.4. Mechanical Property of the PI-ZIF Membrane. Mechanical property is another important property of the nanofibrous membrane. The most common technique to investigate mechanical property is the tensile test. Figure 4a presents the stress−strain curves of the PI-ZIF membranes.

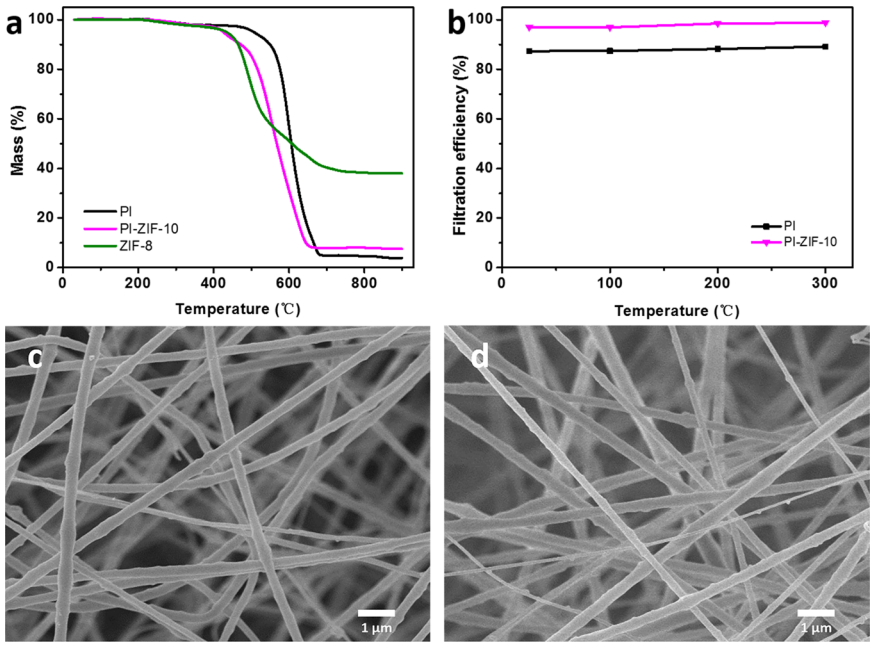

Figure 3. (a) TG curves of PI and PI-ZIF membranes. (b) $PM_{2.5}$ filtration efficiency of PI-ZIF membranes after heat treatment at different temperatures for 1 h. SEM images of PI-ZIF-10 nanofibers (c) without heat treatment and (d) after heat treatment at 300 °C for 1 h.

DOI: 10.1021/acsami.8b22415
ACS Appl. Mater. Interfaces 2019, 11, 11904−11909

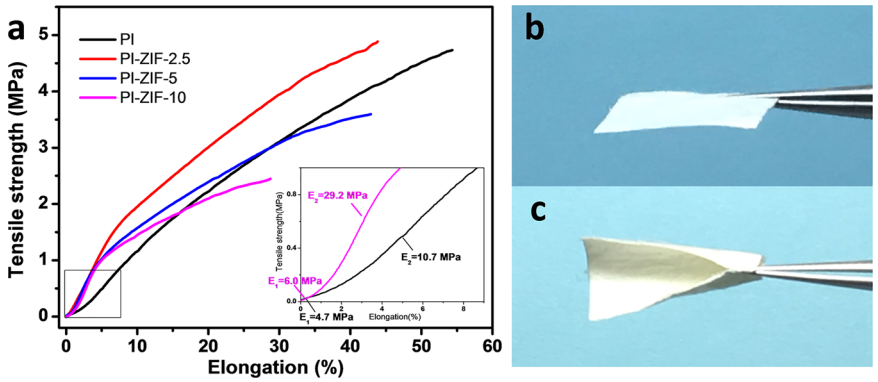

Figure 4. (a) Stress−strain curves of PI/PI-ZIF membranes. The inset shows magnification of the initial part of the stress−strain curve to illustrate modulus variations. (b) Display of PI-ZIF membrane rigidity. (c) Display of PI-ZIF membrane flexibility.

With the increase of the ZIF content, the tensile strength and elongation of PI-ZIF membranes show a weakening trend in whole. When the content of ZIF was up to 20 wt %, the PI-ZIF membrane could not be transferred from the collector due to its poor robustness. It was also found that PI-ZIF-2.5 exhibited a higher tensile strength. With the introduction of ZIF-8, the rigidity of the membrane increased remarkably at the initial stage of deformation. This significant increase of rigidity can be noticed from stress−strain curves, as shown in the inset of Figure 4a. At the initial stretching stage, the fibers oriented along the stretching direction and deformed easily. The moduli of membranes were low, 6.0 MPa for PI-ZIF-10 and 4.7 MPa for PI. With continuous stretching, the fibers realigned in the stretching direction and deformed difficultly. The moduli of membranes increased to 29.2 and 10.7 MPa, respectively.[37] Such high modulus at the initial stage of deformation endows the membrane with antideformation and free-standing ability, as shown in Figure 4b. Meanwhile, the PI-ZIF membrane with increased rigidity still remains flexible enough, as shown in Figure 4c.

4. CONCLUSIONS

The PI-ZIF membranes were successfully prepared via a simple electrospinning process. Upon addition of ZIF-8, the fiber surface became rough and ultrathin fibers appeared. Benefitting from the increase of surface area and multifunctionalization of ZIF-8, the PI-ZIF membrane can achieve high-efficiency filtration ($PM_{2.5}$, 96.6 ± 2.9%). It also has excellent thermal stability, and both the filtration efficiency and morphology can remain unchanged even if the heat treatment temperature is up to 300 °C. Besides, the PI-ZIF membranes show satisfactory mechanical property (rigidity and flexibility), transmittance, and pressure drop. The PI-ZIF membrane with excellent comprehensive performances shows a promising application for $PM_{2.5}$ capture, especially in harsh conditions.

■ ASSOCIATED CONTENT

Supporting Information

The Supporting Information is available free of charge on the ACS Publications website at DOI: 10.1021/acsami.8b22415.

Figure S1, synthetic route of 6FDA−BDAF; Figure S2, XRD patterns of ZIF-8 and ZIF-8 after heat treatment under 300 °C for 1 h and the simulated XRD pattern of ZIF-8; Figure S3, SEM image of ZIF-8 and its particle diameter distribution; Figure S4, schematic illustration of the setup for filtration efficiency and pressure drop measurement; Figure S5, XRD patterns of PI and PI-ZIF membranes; Figure S6, EDS elemental mapping of the PI-ZIF-10 membrane (PDF)

■ AUTHOR INFORMATION

Corresponding Authors

*E-mail: wjt@buaa.edu.cn (J.W.).
*E-mail: liujg@cugb.edu.cn (J.L.).

ORCID

Juntao Wu: 0000-0003-3665-7402

Notes

The authors declare no competing financial interest.

■ ACKNOWLEDGMENTS

The work is financially supported by the National Natural Science Foundation of China (Nos. 51673009 and 51373007), the National Key Research and Development Program of China (No. 2016YFC0303700), the Fundamental Research Funds for the Central Universities, and the SRF for ROCS, SEM.

■ REFERENCES

(1) Brook, R. D.; Urch, B.; Dvonch, J. T.; Bard, R. L.; Speck, M.; Keeler, G.; Morishita, M.; Marsik, F. J.; Kamal, A. S.; Kaciroti, N.; et al. Insights into the mechanisms and mediators of the effects of air pollution exposure on blood pressure and vascular function in healthy humans. *Hypertension* **2009**, *54*, 659−667.

(2) Chan, C. K.; Yao, X. Air pollution in mega cities in China. *Atmos. Environ.* **2008**, *42*, 1−42.

(3) Huang, R.-J.; Zhang, Y.; Bozzetti, C.; Ho, K.-F.; Cao, J.-J.; Han, Y.; Daellenbach, K. R.; Slowik, J. G.; Platt, S. M.; Canonaco, F.; et al. High secondary aerosol contribution to particulate pollution during haze events in China. *Nature* **2014**, *514*, 218.

(4) Kim, K.-H.; Kabir, E.; Kabir, S. A review on the human health impact of airborne particulate matter. *Environ. Int.* **2015**, *74*, 136−143.

(5) Pope, C. A.; Burnett, R. T.; Krewski, D.; Jerrett, M.; Shi, Y.; Calle, E. E.; Thun, M. J. Cardiovascular Mortality and Exposure to Airbourne Fine Particulate Matter and Cigarette Smoke: Shape of the Exposure-Response Relationship. *Circulation* **2009**, *120*, 941−948.

(6) Song, Y.; Wang, X.; Maher, B. A.; Li, F.; Xu, C.; Liu, X.; Sun, X.; Zhang, Z. The spatial-temporal characteristics and health impacts of ambient fine particulate matter in China. *J. Cleaner Prod.* **2016**, *112*, 1312−1318.

(7) Liu, C.; Hsu, P.-C.; Lee, H.-W.; Ye, M.; Zheng, G.; Liu, N.; Li, W.; Cui, Y. Transparent air filter for high-efficiency PM 2.5 capture. *Nat. Commun.* **2015**, *6*, No. 6205.

DOI: 10.1021/acsami.8b22415
ACS Appl. Mater. Interfaces 2019, 11, 11904−11909

(8) Huang, X. C.; Lin, Y. Y.; Zhang, J. P.; Chen, X. M. Ligand-directed strategy for zeolite-type metal-organic frameworks: zinc (II) imidazolates with unusual zeolitic topologies. *Angew. Chem., Int. Ed.* **2006**, *45*, 1557−1559.
(9) Park, K. S.; Ni, Z.; Côté, A. P.; Choi, J. Y.; Huang, R.; Uribe-Romo, F. J.; Chae, H. K.; O'Keeffe, M.; Yaghi, O. M. Exceptional chemical and thermal stability of zeolitic imidazolate frameworks. *Proc. Natl. Acad. Sci. U. S. A.* **2006**, *103*, 10186−10191.
(10) Zhou, H.-C. "Joe"; Kitagawa, S. Metal-organic frameworks (MOFs). *Chem. Soc. Rev.* **2014**, *43*, 5415−5418.
(11) Zhang, Y.; Yuan, S.; Feng, X.; Li, H.; Zhou, J.; Wang, B. Preparation of nanofibrous metal-organic framework filters for efficient air pollution control. *J. Am. Chem. Soc.* **2016**, *138*, 5785−5788.
(12) Chen, Y.; Zhang, S.; Cao, S.; Li, S.; Chen, F.; Yuan, S.; Xu, C.; Zhou, J.; Feng, X.; Ma, X.; et al. Roll-to-Roll Production of Metal-Organic Framework Coatings for Particulate Matter Removal. *Adv. Mater.* **2017**, *29*, No. 1606221.
(13) Bai, F.; Wu, J.; Gong, G.; Guo, L. Biomimetic "cactus spine" with hierarchical groove structure for efficient fog collection. *Adv. Sci.* **2015**, *2*, No. 1500047.
(14) Huang, C.; Chen, S.; Reneker, D. H.; Lai, C.; Hou, H. High-Strength Mats from Electrospun Poly (p-Phenylene Biphenyltetracarboximide) Nanofibers. *Adv. Mater.* **2006**, *18*, 668−671.
(15) Zhang, R.; Liu, C.; Hsu, P.-C.; Zhang, C.; Liu, N.; Zhang, J.; Lee, H. R.; Lu, Y.; Qiu, Y.; Chu, S.; et al. Nanofiber air filters with high-temperature stability for efficient PM2.5 removal from the pollution sources. *Nano Lett.* **2016**, *16*, 3642−3649.
(16) Wang, Z.; Wang, D.; Zhang, S.; Hu, L.; Jin, J. Interfacial design of mixed matrix membranes for improved gas separation performance. *Adv. Mater.* **2016**, *28*, 3399−3405.
(17) Jin, R.; Bian, Z.; Li, J.; Ding, M.; Gao, L. ZIF-8 crystal coatings on a polyimide substrate and their catalytic behaviours for the Knoevenagel reaction. *Dalton Trans.* **2013**, *42*, 3936−3940.
(18) Liu, C.; Wu, Y.-n.; Morlay, C.; Gu, Y.; Gebremariam, B.; Yuan, X.; Li, F. General Deposition of Metal−Organic Frameworks on highly adaptive organic−inorganic hybrid electrospun fibrous substrates. *ACS Appl. Mater. Interfaces* **2016**, *8*, 2552−2561.
(19) Quirós, J.; Boltes, K.; Aguado, S.; de Villoria, R. G.; Vilatela, J. J.; Rosal, R. Antimicrobial metal−organic frameworks incorporated into electrospun fibers. *Chem. Eng. J.* **2015**, *262*, 189−197.
(20) Lu, A. X.; McEntee, M.; Browe, M. A.; Hall, M. G.; DeCoste, J. B.; Peterson, G. W. MOFabric: Electrospun nanofiber mats from PVDF/UiO-66-NH2 for chemical protection and decontamination. *ACS Appl. Mater. Interfaces* **2017**, *9*, 13632−13636.
(21) Bechelany, M.; Drobek, M.; Vallicari, C.; Chaaya, A. A.; Julbe, A.; Miele, P. Highly crystalline MOF-based materials grown on electrospun nanofibers. *Nanoscale* **2015**, *7*, 5794−5802.
(22) Cravillon, J.; Nayuk, R.; Springer, S.; Feldhoff, A.; Huber, K.; Wiebcke, M. Controlling zeolitic imidazolate framework nano- and microcrystal formation: insight into crystal growth by time-resolved in situ static light scattering. *Chem. Mater.* **2011**, *23*, 2130−2141.
(23) Cravillon, J.; Münzer, S.; Lohmeier, S.-J.; Feldhoff, A.; Huber, K.; Wiebcke, M. Rapid room-temperature synthesis and characterization of nanocrystals of a prototypical zeolitic imidazolate framework. *Chem. Mater.* **2009**, *21*, 1410−1412.
(24) Dai, X.; Li, X.; Wang, X. Morphology controlled porous poly (lactic acid)/zeolitic imidazolate framework-8 fibrous membranes with superior PM2.5 capture capacity. *Chem. Eng. J.* **2018**, *338*, 82−91.
(25) Lee, M. J.; Hamid, M. R. A.; Lee, J.; Kim, J. S.; Lee, Y. M.; Jeong, H.-K. Ultrathin zeolitic-imidazolate framework ZIF-8 membranes on polymeric hollow fibers for propylene/propane separation. *J. Membr. Sci.* **2018**, *559*, 28−34.
(26) Pant, H. R.; Bajgai, M. P.; Nam, K. T.; Seo, Y. A.; Pandeya, D. R.; Hong, S. T.; Kim, H. Y. Electrospun nylon-6 spider-net like nanofiber mat containing TiO2 nanoparticles: a multifunctional nanocomposite textile material. *J. Hazard. Mater.* **2011**, *185*, 124−130.
(27) Lee, H. K.; Jeong, E. H.; Baek, C. K.; Youk, J. H. One-step preparation of ultrafine poly (acrylonitrile) fibers containing silver nanoparticles. *Mater. Lett.* **2005**, *59*, 2977−2980.
(28) Jing, L.; Shim, K.; Toe, C. Y.; Fang, T.; Zhao, C.; Amal, R.; Sun, K.-N.; Kim, J. H.; Ng, Y. H. Electrospun polyacrylonitrile-ionic liquid nanofibers for superior PM2.5 capture capacity. *ACS Appl. Mater. Interfaces* **2016**, *8*, 7030−7036.
(29) Zhang, R.; Liu, C.; Zhou, G.; Sun, J.; Liu, N.; Hsu, P.-C.; Wang, H.; Qiu, Y.; Zhao, J.; Wu, T.; et al. Morphology and property investigation of primary particulate matter particles from different sources. *Nano Res.* **2018**, *11*, 3182−3192.
(30) Gong, G.; Zhou, C.; Wu, J.; Jin, X.; Jiang, L. Nanofibrous adhesion: The twin of gecko adhesion. *ACS Nano* **2015**, *9*, 3721−3727.
(31) Li, P.; Zong, Y.; Zhang, Y.; Yang, M.; Zhang, R.; Li, S.; Wei, F. In situ fabrication of depth-type hierarchical CNT/quartz fiber filters for high efficiency filtration of sub-micron aerosols and high water repellency. *Nanoscale* **2013**, *5*, 3367−3372.
(32) Yeom, B. Y.; Shim, E.; Pourdeyhimi, B. Boehmite nanoparticles incorporated electrospun nylon-6 nanofiber web for new electret filter media. *Macromol. Res.* **2010**, *18*, 884−890.
(33) Gu, G. Q.; Han, C. B.; Lu, C. X.; He, C.; Jiang, T.; Gao, Z. L.; Li, C. J.; Wang, Z. L. Triboelectric nanogenerator enhanced nanofiber air filters for efficient particulate matter removal. *ACS Nano* **2017**, *11*, 6211−6217.
(34) Zhang, S.; Liu, H.; Yu, J.; Luo, W.; Ding, B. Microwave structured polyamide-6 nanofiber/net membrane with embedded poly (m-phenylene isophthalamide) staple fibers for effective ultrafine particle filtration. *J. Mater. Chem. A* **2016**, *4*, 6149−6157.
(35) Ye, H.; Li, J.; Lin, Y.; Chen, J.; Chen, C. Synthesis of polyimides containing fluorine and their pervaporation performances to aromatic/aliphatic hydrocarbon mixtures. *J. Macromol. Sci., Part A: Pure Appl. Chem.* **2008**, *45*, 172−178.
(36) Jusoh, N.; Yeong, Y. F.; Cheong, W. L.; Lau, K. K.; Shariff, A. M. Facile fabrication of mixed matrix membranes containing 6FDA-durene polyimide and ZIF-8 nanofillers for CO2 capture. *J. Ind. Eng. Chem.* **2016**, *44*, 164−173.
(37) Gong, G.; Gao, K.; Wu, J.; Sun, N.; Zhou, C.; Zhao, Y.; Jiang, L. A highly durable silica/polyimide superhydrophobic nanocomposite film with excellent thermal stability and abrasion-resistant performance. *J. Mater. Chem. A* **2015**, *3*, 713−718.

DOI: 10.1021/acsami.8b22415
ACS Appl. Mater. Interfaces 2019, 11, 11904−11909